OPEN ACCESS

University of BRISTOL

Peer reviewed version

Link to published version (if available):
10.1016/j.jhydrol.2019.01.070

Link to publication record in Explore Bristol Research

PDF-document

University of Bristol - Explore Bristol Research
General rights

Using δ^{13}C to reveal the importance of different water transport pathways in two nested karst basins, Southwest China

Zhuo Hao [1,2], Yang Gao [1,2*], Mingzhen Ma [1,2], Sophie M. Green [3], Jing Wang [1,2], Xianwei Song[1,2], Jennifer A. J. Dungait[3], Penny J. Johnes[4], Bailian Xiong[5], Timothy A. Quine[3], Xiaomin Sun [1,2*], Xuefa Wen [1,2], Nianpeng He[1,2]

[1] Key Laboratory of Ecosystem Network Observation and Modeling, Institute of Geographic Sciences and Natural Resources Research, CAS, Beijing 100101, P. R. of China; [2] College of Resources and Environment, University of Chinese Academy of Sciences, Beijing, 100190, P. R. of China; [3] Geography, CLES, Amory Building, University of Exeter, Rennes Drive, Exeter EX4 4RJ UK; [4] School of Geographical Sciences, University of Bristol, University Road, Bristol BS8 1SS, UK; [5] College of Resources and Environment, Zunyi Normal College, Zunyi, Guizhou, P. R of China

Abstract: This study used carbon (C) isotope sourcing to determine transport processes of dissolved inorganic carbon (DIC) from the land surface to river catchments in Southwest China. Both nested karst watersheds investigated (Chenqi and Houzhai) are representative of typical karst landform environments (e.g., primary

[*] Corresponding author

E-mail: gaoyang@igsnrr.ac.cn; sunxm@igsnrr.ac.cn

forest, secondary forest, and farmland). We measured DIC concentrations and the $\delta^{13}C$ values of rainfall, river water, groundwater, soil, and plants. To do so, we used IsoSource (a Visual Basic program) to determine source partitioning over time (seasonal) and across the two nested watersheds. In 2017, the mean DIC concentration was 0.06 ± 0.03 mmol L^{-1} and the rainfall $\delta^{13}C_{DIC}$ value was -14.4‰ $\pm$ 1.9‰. We found similar DIC concentrations in the surface and groundwater of both watersheds, ranging from 0.20 to 0.71 mmol L^{-1} (seasonal) and from -3.7‰ to -9.4‰ ($\delta^{13}C_{DIC}$) in the Chenqi catchment and from 0.33 to 0.60 mmol L^{-1} (seasonal) and from -10.3‰ to -6‰ ($\delta^{13}C_{DIC}$) in the Houzhai watershed. The average $\delta^{13}C$ values of soil and local plants were -24.6 ± 1.4‰ and -28.9 ± 1.2‰ in the Chenqi catchment and -25.8 ± 0.9‰ and -27.2 ± 1.8‰ in Houzhai watershed, respectively. In addition, carbonate bedrock and groundwater were the main sources of surface water in the Chenqi and Houzhai nested watersheds, both being greater than 30%. Source percentages were ~20% from atmospheric deposition and ~10% from soil. Furthermore, HCO_3^- was the predominant form of DIC (pH values > 8), and the contribution rates of dissolved carbonate minerals (HCO_3^-) were approximately 10.4% and 19.6% in the Chenqi catchment and the Houzhai watershed, respectively.

Keywords: carbon cycle; source partition; hydrological pathway; catchment

1. Introduction

Continual increases in atmospheric carbon dioxide (CO_2) that result in global warming and associated climate changes necessitate a deeper understanding of global

43   carbon (C) cycles (Huang et al., 2015; Zhao et al., 2015; Shin et al., 2011; Liu et al.,

44   2010). Rivers play the leading role in transporting C from terrestrial to marine

45   ecosystems in the global carbon cycle, being the main conduit of dissolved inorganic

46   carbon (DIC) from the land surface to the oceans (McClanahan et al., 2016).

47   Compared to organic and particulate fractions, DIC concentrations can provide more

48   information on C sources and processes involved in riverine C cycles (Li et al., 2010;

49   Cao et al., 2016; Brunet et al., 2009; Wachniew, 2006). The approximate global C flux

50   from DIC through river transport is 0.4×10^{15} gC yr^{-1}, representing ~50% of the total

51   C flux (Cole et al., 2007).

52   DIC concentrations are influenced by water-air CO_2 exchange processes,

53   hydrologic inputs, vegetation, and carbonate weathering (McClanahan et al., 2016;

54   Shin et al., 2011; Tobias and Böhlke, 2011; Brunet et al., 2009). Sources of DIC in

55   river water include inputs from soil CO_2 (through groundwater), atmospheric CO_2

56   exchange, planktonic respiration, chemical weathering, and the dissolution of

57   carbonate rocks. Recent studies have used stable isotopes to trace DIC sources which

58   are usually characterized by $\delta^{13}C_{DIC}$ values. Each DIC source has a different $\delta^{13}C_{DIC}$

59   isotopic signature (from -26‰ to -9‰ for soil organic matter (SOM) (Wang et al.,

60   2017a), -8‰ to -6‰ for atmospheric CO_2 and approximately 0‰ for carbonate rocks

61   (Brunet et al., 2005). Moreover, C isotopes are used to assess riverine C

62   transformation as well as follow the riverine DIC transport into oceans (Zeng et al,

63   2015 Brunet et al., 2005; Deirmendjian and Abril, 2018; Hu et al., 2017; Ye et al.,

64   2017). Monitoring changes in spatial and temporal DIC concentrations and $\delta^{13}C_{DIC}$

values from inland water systems can provide a better understanding of C sources. At the same time, this approach is useful in revealing reaction pathways and transportation processes which would be difficult to discern with the normative carbonate systems involved in C cycling in freshwater systems (Cao et al., 2016; Tallini et al., 2014).

Approximately 67% of the global DIC in rivers is known to originate from soil CO_2 through C_3 plants, the typical photosynthetic pathway (van Geldern et al., 2015). C_3 plants have $\delta^{13}C$ values that range from -22‰ to -30‰, with an average approximate value of -27‰ (Marx et al., 2018; van Geldern et al., 2015). Along with photosynthesis, the main soil CO_2 transport pathways include rivers and streams. In stream zones, the contribution of groundwater to water flow is significant and the input of DIC-containing groundwater is derived from soil CO_2. Soil CO_2 tends to contain lower $\delta^{13}C_{DIC}$ values in river water because soil CO_2 mainly derives from the microbial degradation of SOM (Shin et al., 2011).

Karst zones are dynamic (McGee et al., 2010), being characterized by surface erosion and extensive subsurface drainage (Song et al., 2017; Chang et al., 2015). Moreover, karst aquifers are apt to form in areas of limestone and dolostone (Williams and Fong, 2010), wherein water is transported under conditions of dissolution. Water transport that takes place in bedrock, sinkholes, sinking streams, and runoff then percolates into groundwater and surface water (Lawhon. 2014). Such areas are environmentally sensitive and are known for their rapid hydrologic and chemical response to changing surface conditions (Yan et al., 2014; Li et al., 2012; Hartmann et

al., 2009; Macpherson et al., 2008). Karst landscapes comprise approximately 11.2%

of the surface area of the planet, namely, approximately 15 million km^2 (Song et al.,

2017; Dürr et al., 2005). Additionally, karst landscapes cover approximately 0.45

million km^2 in Southwest China (Yan et al., 2012). However, karst desertification (i.e.,

total soil loss) has increasingly become a serious problem in this region and could

potentially become a global problem (e.g., changing climatic patterns) (Song et al.,

2017).

Guizhou Province is suitable to study karst environments being located in the

center of the South China Karst, the largest karst area in the world (Liao et al., 2015;

Wang et al., 2017b; Zeng et al., 2015). Moreover, karst water resources account for 80%

of the total water resources in this province (Li et al., 2018; Lu, 2007). This

subtropical region has abundant rainfall (with an average of 1340 mm) as well as

distinct rainy (May to August) and dry seasons. In addition, the surface-groundwater

hydraulic system is a typical karst system, which facilitates the study of

rainfall-driven hydrological C processes and will help in our understanding of C

transport pathways and their implications. Accordingly, the objective of this study was

to determine the importance of different transport pathways in surface and

groundwater in a karst river basin (comprised of nested karst watersheds) using

$\delta^{13}C_{DIC}$ to trace C sources. However, the present researches generally focused on

relationship between surface water and groundwater or C sources of groundwater in

karst watersheds (Zeng et al., 2015; Deirmendjian and Abril 2018; Marx et al. 2018).

Therefore, the novelty of our research lies in using $\delta^{13}C_{DIC}$ from precipitation, plant,

109   soil to water throughout the whole watershed to trace the C transport and analyzing

110   seasonal differences in C sources, thereby contributing to the further understanding of

111   C transport and storage in large karst basins.

112   **2. Materials and Methods**

113   **Study site**

114   This study was conducted in the Houzhai watershed (80.65 km^2) (26°15′ N;

115   105°41′ E) located in Guizhou Province, Southwest China (Figure 1a). The bedrock

116   type in the drainage area is predominantly limestone and dolomite of the Middle

117   Triassic Guanling Formation (Liu et al., 2010a, 2010b; Zhao et al., 2010). The

118   drainage basin ranges in altitude between 1218 and 1585 m above mean sea level

119   (AMSL). This region is under the influence of a subtropical monsoon climate with an

120   annual mean temperature of 15.2°C (Yan et al., 2012). Annual average precipitation is

121   1314.6 mm, and 85% of rainfall occurs during the rainy season (from May to

122   October) (Yan et al., 2012). Tianlong Mountain (26°14′48″ N; 105°45′51″ E) is

123   located within the Houzhai watershed. The area of this mountain is 0.5 km^2 and its

124   altitude is 1460 m AMSL (Figure 1a). The mountain is covered by nearly 100%

125   natural forests where the average tree height is 6.26 m, the average shrub layer is 1.3

126   m, and the average herbaceous layer is 0.4 m. In the study area, the black "residual"

127   soil from 50 to 80 cm deep follows the Chinese soil taxonomic system. The Chenqi

128   catchment (105°42′ E; 26°14′ N), which has an area of 1.31 km^2, is nested within the

129   Houzhai watershed (see Figure 1b). Annual mean temperature is 14.2°C, mean

130   precipitation is 1336 mm, and the altitude ranges from 1338 to 1491 m AMSL. The

131 land-use type of the Chenqi catchment is predominantly agricultural, including dry

132 crops (i.e., maize; 56%), rice paddies (14%), abandoned areas dominated by shrubs

133 (23%), and fruit trees (7%).

134 **Water sampling**

135 Surface and groundwater samples were collected from the Houzhai watershed and

136 the Chenqi catchment twice a month from June 28th, 2016, to May 23rd, 2017. Figure

137 1b shows the 10 sampling locations in the Houzhai watershed: No. 1 is comprised of

138 three sampling point (No. 1 surface water, No. 1G groundwater, and No. 1M the

139 surface–groundwater mixed sampling points) and No. 2 to No. 10 are all comprised of

140 surface water sampling points. Figure 1c shows that the Chenqi catchment is

141 comprised of four groundwater sampling points (No. 1G, No. 3G, No. 6G, and No.

142 8G), six surface water sampling points (No. 1 through No. 6), and one

143 surface-groundwater mixed sampling point (No. 7).

144 Samples were collected in 100 mL polyethylene plastic bottles and stored prior to

145 analysis (4°C). Samples were filtered through a 0.45 μm membrane filter (Millipore)

146 (Jiangsu Jiuding Group Co., Ltd., China). Water samples used to determine DIC,

147 taken from the Millipore membranes, were thereafter heated to 80°C and maintained

148 at this temperature for 8 h to remove impurities. We determined DIC using a Vario

149 TOC Analyzer (Elementar, Langenselbold, Hesse, Germany) and $\delta^{13}C_{DIC}$ using a

150 Finnigan MAT-252 mass spectrometer (Thermo Fisher Scientific, Darmstadt, Hesse,

151 Germany) We measured K^+, Ca^{2+}, SiO_2, Na^+, and Mg^{2+} using an inductively coupled

152 plasma optical emission spectrometer (ICP-OES) (Thermo Fisher Scientific,

153   Darmstadt, Hesse, Germany) and Cl$^-$ and SO$_4^{2-}$ using an ion chromatograph (Thermo

154   Scientific Aquion IC, USA). We measured electrical conductivity (COND), redox

155   potential (ORP), total dissolved solids (TDS), and water acidity (pH) using Ultrameter

156   Ⅱ pH meters (Myron L company, Carlsbad, CA, USA). To collect rainfall samples,

157   we installed a rain gauge on the roof of the station near No.1 sampling point in the test

158   area of Houzhai watershed.

Plant and soil sampling

159

160   We collected plant and soil samples from the Chenqi catchment and the Tianlong

161   Mountain in July 2016. For the Tianlong Mountain, we chose four height gradients (A,

162   B, C, and D), and each height gradient was divided into four separate soil layers (0–10,

163   10–30, 30–50, and 50–100 cm) for soil sampling. Plant samples were collected from

164   leaves, roots and twigs of different tree species. In the Chenqi catchment, two

165   transects were established (Figure 1d) downslope on the hillside. Four quadrats were

166   established on each transect from which plant and soil samples were collected. A total

167   of 18 soil samples were collected from farmland, orchard, and forest land use types.

168   Continuous soil cores were taken and subsampled at depth intervals of S1 (0–10 cm),

169   S2 (10–30 cm), S3 (30–50 cm), and S4 (50–100 cm). Plant samples were collected as

170   mixed samples according to type (i.e., tree, shrub, or herb). These plant samples were

171   oven-dried at 60°C and then ground to <150 μm. Two milligrams of the subsamples

172   were prepared for stable isotope analysis, and soil samples were then air-dried and

173   ground to 150 μm. Finally, subsamples (3 g) were acidified (5% HCl) and then

174   analyzed for δ^{13}C using the Finnigan MAT-252 mass spectrometer.

175 **Statistical analysis**

176 **Isotopic mixing model**

177   Utilizing one isotope system and three sources, we used the following mass balance

178 equations to determine the proportions (f_A, f_B, and f_c) of isotopic signature sources (δ_A,

179 δ_B, and δ_c), which coincide with the observed signatures of the mixture (δ_M):

180    $\delta_M = f_A\delta_A + f_B\delta_B + f_C\delta_C$

181    $1 = f_A + f_B + f_C$

182   however, with n (A, B, C, …) isotope systems and >n+1 sources, we were still

183 able to apply the requirement for mass balance conservation to determine multiple

184 combinations of source proportions that offer feasible solutions (Phillips and Gregg,

185 2003; Hao et al., 2018).

186   Stable isotope compositions of DIC in water, soil, and plant samples were

187 expressed as conventional delta notations, the difference between measured ratios of

188 the samples and references over the measured ratios of the references:

189    $\delta^{13}C_{DIC}(‰) = \left(\dfrac{R_{Sample} - R_{Standard}}{R_{Standard}} \right) \times 1000$

190 where R_{sample} and $R_{standard}$ represent $^{13}C/^{12}C$ in the samples and the standard references.

191 Carbon isotope data were reported on the Vienna Pee Dee Belemnite (VPDB) (‰)

192 scale, with a standard deviation (1σ) of 0.15‰ (Zhao et al., 2015).

193   Principal component analysis (PCA) and factor analysis were used with SPSS 17.0

194 software (SPSS Inc., Chicago, IL, the USA). The model outputs presented feasible

195 ranges of isotope contributions given that the mass balance with qualitative statistics

196 were calculated by IsoSource.

197

3 Results

3.1 Seasonal hydrochemical variations

Figure 2a shows the seasonal variation of pH ranges in the Houzhai watershed. The pH ranges were highest in autumn, namely, from 8.6 to 9.1 (except for the outliers) and lowest in summer, namely, from 8.3 to 8.5, and from 8.2 to 8.7 and from 8.2 to 8.5 in winter and spring, respectively. Figure 2b shows the seasonal variation of pH in the Chenqi catchment. Compared to the Houzhai watershed, pH ranges in the Chenqi catchment were narrow with the exception of spring. The highest values occurred in summer, namely, from 8.4 to 9.1 (except for the outliers) and the lowest in spring (from 7.8 to 8.2). Autumn and winter pH values were similar.

Figure 2c shows linear relationships between pH, COND, TDS, and ORP of 21 rainfall events, respectively. We found that COND and TDS values were positively correlated to pH values, while ORP values were negatively correlated to pH values. Table 1 shows the seasonal variation in water quality parameters of surface water, groundwater, and mixed sampling points in the Houzhai and Chenqi nested watersheds. As Table 1 shows, seasonal variation of ORP and pH in surface water, groundwater and mixed water were only slightly different in Houzhai watershed, while ORP values were much higher in summer and spring in Chenqi catchment. Furthermore, pH values in the Houzhai watershed were lower than Chenqi catchment with the exception of spring. Compared to other seasons, only COND and TDS values were higher in surface water than groundwater in the Houzhai watershed. Additionally, COND and TDS values in Chenqi were obviously

higher than the Houzhai watershed all year round. However, ORP values were particularly lower in the Chenqi catchment compared to the Houzhai watershed with the exception of spring in surface water.

3.2 Variations in dissolved inorganic carbon and $\delta^{13}C$

We collected data on 21 rainfall events from June 28th, 2016, to May 23rd, 2017, and found that DIC values for eight rain events were nearly 0 mmol L^{-1}. As Figure 3a shows, seasonal changes were significant, where the maximum concentration was 0.09 mmol L^{-1} in the spring of 2017 and the minimum concentration was nearly 0 mmol L^{-1} in the autumn of the same year. The average DIC concentration for all rain events was 0.02 ± 0.03 mmol L^{-1}. Additionally, DIC concentrations for rainfall events in 2017 were significantly higher compared to 2016, where the average DIC concentration for rain events from January to May 2017 was 0.06 ± 0.03 mmol L^{-1}. Figure 3b shows variation in $\delta^{13}C$ values for 11 rain events throughout 2016 to 2017. Seasonal variation was not obvious, wherein the maximum was -12.3‰ in the spring of 2017 and the minimum was -18.3‰ in the autumn of 2016. The average for all 11 rain events was -14.4‰ $\pm$ 1.9‰.

As Figure 4a shows, DIC concentrations in the Houzhai watershed ranged from 0.33 to 0.48 mmol L^{-1} during the summer, from 0.33 to 0.49 mmol L^{-1} during the autumn, from 0.39 to 0.58 mmol L^{-1} during the winter, and from 0.37 to 0.57 mmol L^{-1} during the spring. We found greater variation in DIC during the winter and spring compared to the summer and autumn. In sampling point No.1, surface water and groundwater exhibited similar variation, and DIC concentrations in groundwater were

241 higher than surface water.

242   Figure 4b shows DIC variation in the Chenqi catchment. We were able to obtain a

243 complete dataset of groundwater sampling points for all four seasons (winter, spring,

244 summer, and autumn). With the exception of No. 8G, namely, the groundwater

245 sampling points from the hilly area, all groundwater sampling points exhibited similar

246 variation, wherein the highest DIC concentration was measured in spring and lowest

247 in autumn. The No. 7 sampling point was also a surface and groundwater mixed

248 sampling point (where No. 6 and No. 6G were combined), and we found little

249 difference in DIC concentrations between surface and groundwater for all four

250 seasons. The maximum DIC concentration in the Chenqi catchment was 0.71 mmol

251 L^{-1}in spring and the minimum was 0.20 mmol L^{-1} in summer.

252   In both watersheds, DIC concentrations between surface water and groundwater

253 were only slightly different. Moreover, we found higher concentrations for both during

254 spring, when the averages were 0.50 and 0.56 mmol L^{-1}, and lower concentrations were

255 measured during autumn, when the averages were 0.39 and 0.41 mmol L^{-1} in the

256 Houzhai and Chenqi nested catchments, respectively. Surface water was abundant in

257 summer due to high rainfall frequency and abated in the autumn and winter, while

258 abundant groundwater was available all year around.

259   Figure 4c shows the 2016–2017 $\delta^{13}C$ values in the Houzhai watershed during the

260 autumn, winter, and spring. The range in variation of $\delta^{13}C$ values was from -10.3‰ to

261 -6‰, and the average $\delta^{13}C$ values in the autumn, winter, and spring were -9.0‰ ± 0.9‰,

262 -8.1‰ ± 1.0‰, and -7.4‰ ± 0.9‰, respectively. $\delta^{13}C$ values were more depleted in

263   autumn and were more enriched in spring, Figure 4d shows that δ^{13}C values in surface

264   water and groundwater of the Chenqi catchment exhibited little difference, wherein the

265   average δ^{13}C values were -7.4‰ ± 2.0‰ in surface water and -7.2‰ ± 2.2‰ in

266   groundwater. Furthermore, different months yielded obviously different values in

267   sampling point No. 6, where the maximum value was -3.7‰ in surface water in August

268   and the minimum value was -9.4‰ in groundwater in August due to frequent rainfall.

269   **3.3 Variation in δ^{13}C values for soil and vegetation**

270   Figure 5a shows the δ^{13}C soil values of the four sampling depths of the different

271   height gradients (from A to D) in the Tianlong Mountain, wherein the lowest values

272   occurred in topsoil at all sampling points. The δ^{13}C values in sampling points B and C

273   exhibited the same trend, namely, the deeper the soil layers were, the more depleted the

274   δ^{13}C values were. The minimum value was -27.0‰ for the 0 to 10 cm soil layer in

275   sampling point A, and the maximum value was -24.0‰ for the 50 to 100 cm soil layer in

276   sampling point B. Figure 5b and 5c show the differences in two transects of a ditch

277   between two hills in the Chenqi catchment. For example, the δ^{13}C value range in CQ-1

278   was from -28.3‰ to -22.6‰ and the δ^{13}C value range in CQ-2 was from -27.6 ‰ to

279   -22.0‰. The averages of CQ-1 in S1 (0–10 cm), S2 (10–30 cm), S3 (30–50 cm), and S4

280   (50–100 cm) were -24.9‰, -24.8‰, -24.2‰, and -24.5‰, respectively, and the averages

281   of CQ-2 were -25.5‰, -24.3‰, -24.7‰, and -24.6‰, respectively. We found that [13]C

282   values were more enriched in the deeper soil layers (10–50 cm).

283   Figure 6a shows the δ^{13}C values of the four plant types in the Tianlong Mountain,

284   which is near sampling point No. 8 in the Houzhai watershed. The highest δ^{13}C value was

285 -24.6‰ (cedar wood) and the lowest $\delta^{13}C$ value was -27.6‰ (*Broussonetia papyrifera*)

286 among the four plant types. Figure 6b shows the mixed samples of trees divided into

287 leaves, twigs, and roots, wherein the average $\delta^{13}C$ values were -30.2‰ ± 0.3‰, -28.7‰ ±

288 0.6‰, and -27.7‰ ± 0.5‰, respectively. Therefore, ^{13}C concentrations increased in the

289 roots of plants.

290

291 **4. Discussion**

292 **4.1 Inorganic river chemistry**

293   Dissolved and particulate C is likely associated with the chemical weathering of

294 basin soil and bedrock (McClanahan et al., 2016). COND is an indicator that reflects

295 ion changes under some conditions. Higher COND values indicate higher ionic

296 concentrations in water bodies, which may stem from the dissolution of carbonate

297 minerals. Both surface water and groundwater in the Chenqi catchment (TDS values:

298 510~723 mg·L^{-1}) were much more carbonate-rich compared to the Houzhai watershed

299 (TDS values: 262~432 mg·L^{-1}) all year around (Table 1). This indicated that there was

300 not only an increase in karst dissolution processes adding to the dissolved constituents

301 in the water, but other potential sources along the surface water path were

302 contributing COND and TDS values in karst water. These potential sources included

303 overland flow and anthropogenic impacts which also have influences on ionic

304 concentrations (COND) especially agricultural activities including potassium, nitrates,

305 and phosphates fertilizers (Lawhon, 2014; Moore et al., 2009).

306   The nature of redox reactions and redox-sensitive aqueous species is quite

307 different from most other reactions in aquifer systems (Liu et al., 2017). Therefore, it

308 is necessary to set a unique redox status indicator in aquifer systems (Kumar and

309 Riyazuddin, 2012). In water, ORP is strongly associated with temperature, pH, salinity,

310 and dissolved oxygen concentrations (Liu et al., 2009; Li et al., 2014). The greater the

311 dissolved oxygen (DO) is, the higher the ORP will be. As Table 1 shows, the Houzhai

312 watershed yielded higher ORP compared to the Chenqi catchment; thus, its living

313 conditions were better suited for aquatic organisms, when considering variations in

314 pH and DO simultaneously.

315 In karst areas, such as the Houzhai and Chenqi nested watersheds, given the

316 abundant carbonate bedrock, carbonates will help remove CO_2 from the system.

317 Under most conditions, CO_2 is consumed because carbonate minerals dissolve in

318 H_2O–CO_2 solutions, and pH will buffer to higher values due to adjustments in

319 relevant reactions (chemical equilibrium).

320 As Figure 2c and Table 1 show, pH values were generally high in the sampling

321 areas, and pH values in the Chenqi catchment were higher than in the Houzhai

322 watershed. The CO_2 that escaped from streams in the Chenqi catchment reacted much

323 more significantly than river water in the Houzhai watershed. Guizhou Province has a

324 rich karst landscape, including carbonates and other minerals; therefore, water quality

325 parameters, such as COND and TDS, are much higher in water than other areas.

326 Moreover, these parameters have a direct effect on pH values in that they are higher

327 than other areas (McClanahan et al., 2016; Lawhon, 2014; Mondal et al., 2010).

328 However, previous literature reported that karst water bodies had been found to have

329 higher pH ranges in general (Hatcher, 2013).

4.2 Using $\delta^{13}C$ values to distinguish between sources of dissolved inorganic

carbon

332 Many internal and external factors, such as soil respiration, carbonate mineral

333 dissolution, atmospheric precipitation, and the pH value of water bodies, etc., have an

334 effect on $\delta^{13}C_{DIC}$ in water catchments (Shin et al., 2011; Doctor et al., 2008). In this

335 study, the average $\delta^{13}C$ values of surface water were lower than groundwater in the

336 Houzhai and Chenqi nested watersheds. This could be explained in that groundwater

337 may be derived more from "old" water in matrix pores that is more enriched in

338 $\delta^{13}C_{DIC}$ due to the longer time required for $CaCO_3$ dissolution to take place, while

339 river water has many sources, including groundwater inputs, atmospheric deposition,

340 soil water, and carbonate reactions. In order to determine $\delta^{13}C$ proportions from

341 various sources, the isotope model that we used to calculate results from IsoSource is

342 provided for the Houzhai and Chenqi nested watersheds (see Figure 7). As it pertains

343 to river water (surface water) and groundwater time spans, atmospheric deposition

344 results are typically taken from long-term monitoring, where, for example, average

345 soil $\delta^{13}C$ values are from -21‰ to -22‰ in karst areas of USA (McClanahan et al.,

346 2016). In China, the average soil $\delta^{13}C$ value is -24‰ (Zhao et al., 2015).

347 In this study, soil water was assumed to be -24‰ and carbonate mineral sources

348 were hypothesized to be 0‰ (Das et al., 2005; Hu et al., 2017; Li et al., 2010). The

349 main sources in the Chenqi catchment were groundwater and carbonate reactions,

350 wherein the mean percentages were 31.7% and 38.1%, respectively; the minimum

351 source was soil water, with a mean percentage of only 10.1% during the summer

352 (Figure 7). In autumn, when stream flows were lower, percentages of groundwater

353 were higher compared to carbonate reactions (Yan et al., 2014; Zhao et al., 2010). The

354 proportion in the Houzhai watershed was similar to that of the Chenqi catchment,

355 wherein the main sources were groundwater and carbonate reactions, which showed

356 little differences between seasons. The mean proportions of the four sources were 32.4%

357 in the autumn and 35.5% in the spring from groundwater, 20.5% in the autumn and

358 18.8% in the spring from atmospheric deposition, 11.4% in the autumn and 10.5% in

359 the winter from soil water, and 35.7% in the autumn and 34.6% in the spring from

360 carbonate reactions. In autumn, rainfall contributed more, which reduced the overall

361 groundwater impact. Furthermore, winter and spring showed little seasonal

362 differences in the difference in Houzhai watershed.

363   Figure7 shows the mean percentage of each source. All values are provided in

364 Table 2, which also summarizes seasonal trends. To present model results more

365 accurately, median values of model averages are provided along with the standard.

366 The median value of carbonate reactions was highest (38% ± 13%) in summer and

367 groundwater was highest (32% ± 24%) in autumn. The lowest DIC source was found

368 in soil water, which likely derived from the interflow of water being infiltrated along

369 slopes within the basin (9% ± 8%) in summer and (11% ± 9%) in the Chenqi

370 catchment in autumn. In summer, rainfall was more frequent and subsequently surface

371 water was more abundant; thus groundwater and soil water were lower than in the

372 autumn. We found little differences between seasons in the Houzhai watershed. The

373 highest mean for all *in situ* carbonate reactions was 36%, and the lowest mean for all

374 soil was 8% as shown in Table 2.

375 **4.3 Influence and contribution rates of carbonate dissolution on dissolved**

376 **inorganic carbon concentrations**

377 River chemistry is strongly influenced by carbonate dissolution, which has an

378 obvious effect on pH value and supplies a large quantity of DIC in the form of

379 bicarbonates (Schulte et al., 2011). The study area lies within the carbonate area of the

380 region, and the distribution of pH in groundwater ranged from 7.9 to 9.0. Therefore,

381 the type of inorganic C in water is predominantly HCO_3^- (Doctor et al., 2007). COND

382 and pH values are shown in Table 1, which were completely consistent for both

383 sampling points. They showed that carbonate minerals control dissolution, including

384 the main DIC components in both the Chenqi catchment and the Houzhai watershed.

385 Cations (Ca^{2+}, Mg^{2+}, K^+, and Na^+) and anions (HCO_3^-, Cl^-, and SO_4^{2-}) were the

386 main ions found in the Chenqi catchment and the Houzhai watershed (Table 3). The

387 Piper diagram reflects not only the chemical composition of river water but also

388 distinguishes between different weathered sources of species composition (Stallard et

389 al., 1983). In the cationic ternary diagram (Figure 8), evaporite mineral weathering

390 products fall on the high Na^++K^+ line, while limestone weathering products fall on

391 Mg^{2+}-Ca^{2+} line. Due to dolomite characteristics, weathering products fall in the

392 middle of the Mg^{2+} and Ca^{2+} (Ca: Mg = 1:1) lines(Li et al., 2010).

393 Furthermore, the weathering products of silicate minerals fall on the Mg^{2+}-Ca^{2+}

394 line, which is relatively biased towards one side of Na^++K^+. In the anion ternary graph,

the weathering material of pure carbonates is primarily HCO_3^-; thus, the data points

fall at the relatively high end of HCO_3^-. The weathering products of evaporated salt

minerals fall on the $Cl^- + SO_4^{2-}$ line, and the proportion is relatively high, while the

weathering of silicate minerals causes both HCO_3^- and SiO_2 to be present in river

systems. In this study, the proportion of Ca^{2+} and Mg^{2+} were higher than $Na^+ + K^+$. In

particular, Ca^{2+}, HCO_3^-, and SO_4^{2-} were obviously higher than Cl^- and Mg^{2+} in the

Chenqi catchment and the Houzhai watershed, which suggested that river water in

these two nested watersheds are controlled by carbonates, silicate minerals, and small

amounts of evaporites.

In order to further quantify the influence of different rock types on the main ions

found in rivers, we used the main ion concentrations (Ca^{2+}, Mg^{2+}, K^+, Na^{2+}, Cl^-, SiO_2,

and HCO_3^-) of surface water in the Chenqi catchment and the Houzhai watershed for

PCA and factor analysis of river water chemistry as shows in Table3 and Figure 9. In

the Chenqi catchment, as Figure 9 shows, the cumulative contribution rate of the first

three variables reached 79.6% (<80%), but eigenvalues from the extraction factor

were less than 1 of the fourth variable, and therefore deleted. Factor 1 was highly

correlated to Ca^{2+}, Mg^{2+}, Na^{2+}, and SiO_2, indicating that the dissolution of silicate

minerals contributes to chemical weathering in the sampling areas. Factor 2 was more

significantly correlated to K^+ and HCO_3^-, and Factor 3 was more significantly

correlated to Cl^- and SO_4^{2-}, indicating that the contribution of dissolved carbonate

minerals was relatively high compared to silicate minerals (Figure 9). Bare carbonate

rocks accounted for almost 75% of the study area, which suggested that carbonate

417 dissolution should play a key role in rock weathering (Cao et al., 2005; Li et al., 2010).

418 In the Houzhai watershed, as Figure 9 shows, the cumulative contribution rate of the

419 first three variables reached 81.2% (>80%), and the relationship between each factor

420 was similar to the Chenqi catchment. The squares of each variable factor load divided

421 by the common variance is the relative variance contribution of dissolution of each

422 type of rock to each variable. After calculations, the contribution rates of dissolved

423 carbonate minerals to HCO_3^- were approximately 10.4% and 19.6% in the Chenqi

424 catchment and the Houzhai watershed, respectively.

425 **4.4 $\delta^{13}C$ characteristics of vegetation and soil**

426 The $\delta^{13}C$ values of the C_3 and C_4 photosynthetic pathway plants were distinctly

427 different, namely, the average value of C_3 plants is -27.1‰ (from -21‰ to -35‰) and

428 the average value of C_4 plants is -13.1‰ (from -10‰ to -14‰) (Rouw et al., 2015). In

429 our study, all plant $\delta^{13}C$ values in the Houzhai watershed were from -24.6‰ to -27.6‰

430 and all plant $\delta^{13}C$ values in the Chenqi catchment were from -27.7‰ to -30.2‰. For

431 CQ-1, soil $\delta^{13}C$ values were more enriched in the deeper soil layers, with an order

432 rank of S1<S2<S4<S3, and the order rank of soil $\delta^{13}C$ values in CQ-2 was S1<

433 S3<S4<S2. The reason for this could potentially be that surface soil is easily

434 transported by rain, promoting nutrient accumulation in deeper soil layers (10–50 cm)

435 in karst areas. The 0–10 cm soil layer in these soil profiles had the lowest $\delta^{13}C$ values

436 of the corresponding profile. This is due to the fact that the top of the soil profile had

437 a relatively large amount of undecomposed plant residue and better preserved plant

438 $\delta^{13}C$ signatures, while underneath the surface soil, due to the uneven distribution of

439   plant roots, different degrees of plant residue decomposition and differences in

440   organic or acid species in the soil itself, etc., could lead to differences in $\delta^{13}C$ soil

441   sample values (Wynn et al., 2006; Wang et al., 2008).

442   The average $\delta^{13}C$ value of SOC for the four soil profiles was -24.6‰±1.4‰ in the

443   Chenqi catchment, with an $\delta^{13}C$ enrichment value of 4‰ compared to the weighted

444   average $\delta^{13}C$ value of local plants (-28.9‰±1.2‰). This trend was also seen in the

445   Houzhai watershed, with an average value of -25.8‰±0.9‰, an increase of nearly 2‰

446   compared to local plants. During isotope fractionation, which occurs through

447   microbial decomposition of organic matter and leads to the uneven distribution of ^{13}C

448   and ^{12}C during the different C phases between reactants and products, there is

449   relatively more ^{12}C in released CO_2, whereas ^{13}C is more prevalent in C derived from

450   microbial biomass, eventually being returned as SOM (Luo and Wang, 2009; Li et al.,

451   2012). Furthermore, even for individual plants, ^{13}C tends to concentrate in root

452   systems followed by twigs and leaves, and this is because the lighter ^{12}C isotope exits

453   plants through transpiration. In order to fully understand C cycling, more research is

454   required on interannual changes, photosynthesis and transpiration of C_3 and C_4 plants,

455   and soil microbial respiration to better understand internal C cycling dynamics that

456   could influence DIC sources, transportation, and storage, which could even lead to an

457   improvement in global C sink estimations (Figure 10).

458

459   **5. Conclusions**

460   Carbonate karst environments may play an indispensable role in the global C

461 budget. Investigations into the impacts of karst watersheds such as C transportation

462 and storage within this system on a local level are vital to understanding the global C

463 cycle. International and domestic academics have provided credible scientific data

464 regarding many aspects of karst watersheds in China. However, additional research is

465 needed for a better comprehensive understanding of DIC and its sources in this type

466 of system. In this study, carbonate reactions and groundwater were the main sources

467 of river water in Houzhai and Chenqi watersheds, whose proportions were both

468 greater than 30% in river water. Sources proportions were influenced by seasonality

469 which related to the frequency of rainfall, especially regarding groundwater and soil

470 water. Furthermore, DIC mainly exists in the form of HCO_3^- in the sampling areas of

471 this study, of which the contribution rate of dissolved carbonate minerals (HCO_3^-) was

472 approximately 10.4%-19.6%. Silicate minerals and evaporites had a negligible effect

473 on DIC in the nested watersheds investigated in this study. The amount of carbonate

474 mineral dissolution had a significant influence on surface water and groundwater (in

475 the form of a C sink) under karst hydrological conditions. Additionally, water-soil and

476 soil-plant processes together comprised the complete karst eco-hydrological C cycle

477 in this study which is not mentioned in other studies at present. More relevant studies,

478 however, are required in order to gain a more comprehensive understanding of

479 biogeochemical cycles in large karst-influenced watersheds.

480 **Acknowledgments**

Research Network, Chinese Academy of Sciences. This study was financially

supported by the National Nature Science Foundation of China (No.41571130043,

41871080 and 31570465) and the Youth Innovation Promotion Association of the

Chinese Academy of Sciences.

References

Brunet, F., Gaiero, D., Probst, J. L., Depetris, P.J., Lafaye, F. G., Stille, P., 2005. delta

C-13 tracing of dissolved inorganic carbon sources in Patagonian rivers

(Argentina). Hydrol Process 19, 3321-3344. https://doi.org/10.1002/hyp.5973.

Brunet, F., Dubois, K., Veizer, J., Ndondo, G. R. N., Ngoupayou, J. R. N., Boeglin, J.

L., Probst, J. L. 2009. Terrestrial and fluvial carbon fluxes in a tropical

watershed: nyong basin, cameroon. Chemical Geology, 265(3), 563-572.

https://doi.10.1016/j.chemgeo.2009.05.020.

Cao, X. X., Wu, P., Han, Z. W., Tu, H., Zhang, S. 2016. Factors controlling the isotope

composition of dissolved inorganic carbon in a karst-dominated wetland

catchment, Guizhou Province, Southwest China, Environmental Earth

Sciences, 75(14), https://doi.Artn 110310.1007/S12665-016-5899-4.

Cole, J. J., Prairie, Y. T., Caraco, N. F., McDowell, W. H., Tranvik, L. J., Striegl, R. G.,

Duarte, C. M., Kortelainen, P., Downing, J. A., Middelburg, J. J., Melack, J.,

2007. Plumbing the global carbon cycle: Integrating inland waters into the

terrestrial carbon budget, Ecosystems, 10(1), 171-184.

https://doi.10.1007/s10021-006-9013-8.

Chang, Y., Wu, J. C., Jiang, G. H. 2015. Modeling the hydrological behavior of a karst

505   spring using a nonlinear reservoir-pipe model, Hydrogeology Journal, 23(5),

506   1-14. https://doi. 10.1007/s10040-015-1241-6.

507 Das, A., Krishnaswami, S., Bhattacharya, S. K., 2005. Carbon isotope ratio of

508   dissolved inorganic carbon (DIC) in rivers draining the Deccan Traps, India:

509   Sources of DIC and their magnitudes. Earth Planet Sc Lett 236, 419-429.

510   https://doi. 10.1016/j.epsl.2005.05.009.

511 Deirmendjian, L., Abril, G., 2018. Carbon dioxide degassing at the

512   groundwater-stream-atmosphere interface: isotopic equilibration and

513   hydrological mass balance in a sandy watershed. J Hydrol 558, 129-143.

514   https://doi. 10.1016/j.jhydrol.2018.01.003.

515 Doctor, D. H., Kendall, C., Sebestyen, S. D., Shanley, J. B., Ohte, N., & Boyer, E. W.

516   2010. Carbon isotope fractionation of dissolved inorganic carbon (dic) due to

517   outgassing of carbon dioxide from a headwater stream. Hydrological Processes,

518   22(14), 2410-2423. https://doi. 10.1002/hyp.6833.

519 Dürr, H. H., Meybeck, M., Dürr, S. H. 2005. Lithologic composition of the earth's

520   continental surfaces derived from a new digital map emphasizing riverine

521   material transfer. Global Biogeochemical Cycles. 19(4).

522   https://doi.10,1029/2005GB002515.

523 Gao, Y., He, N. P., Wang, Q. F., Miao, C. Y. 2013. Increase of External Nutrient Input

524   Impact on Carbon Sinks in Chinese Coastal Seas. Environmental Science &

525   Technology, 47(23), 13215-13216. https://doi. 10.1021/es4045743.

526 Gao, Y., Yu, G. R., Yang, T. T., Jia, Y. L., He, N. P., Zhuang, J. 2016. New insight into

527   global blue carbon estimation under human activity in land-sea interaction area:

528   A case study of China. Earth-Science Reviews, 159, 36-46. https://doi.

529   10.1016/j.earscirev.2016.05.003.

530   Hao, Z., Gao, Y., Sun, X. M., Wen, X. F. 2018. Differential isotopic characteristics of

531   eco-hydrologic processes in a subtropical watershed, China. Ecohydrology,

532   11(4). https://doi. Unsp E194410.1002/Eco.1944.

533   Hartmann, J., Jansen, N., Durr, H. H., Kempe, S., Kohler, P. 2009. Global

534   CO_2-consumption by chemical weathering: What is the contribution of highly

535   active weathering regions? Global and Planetary Change, 69(4), 185-194.

536   https://doi.10.1016/j.gloplacha.2009.07.007.

537   Hatcher, B. E., 2013. Sources of CO_2 Controlling the Carbonate Chemistry of the

538   Logsdon River, Mammoth Cave, Kentucky. M.S. Thesis, Department of

539   Geography and Geology, Western Kentucky University, Bowling Green, KY.

540   Hu, Y., Lu, Y.H., Liu, C.K., Shang, P., Liu, J., Zheng, C.M. 2017. Sources and

541   Dynamics of Dissolved Inorganic Carbon, Nitrogen, and Phosphorus in a

542   Large Agricultural River Basin in Arid Northwestern China. Water, 9(6).

543   https://doi. Artn 415.

544   Huang, F., Zhang, C. L., Xie, Y. C., Li, L., Cao, J. H. 2015. Inorganic carbon flux and

545   its source in the karst catchment of Maocun, Guilin, China. Environmental

546   Earth Sciences, 74(2), 1079-1089. https://doi.10.1007/s12665-015-4478-4.

547   Huang, Q. B., Qin, X. Q., Yang, Q. Y., Liu, P. Y., Zhang, J. S. 2016. Identification of

548   dissolved sulfate sources and the role of sulfuric acid in carbonate weathering

549   using delta C-13(DIC) and delta S-34 in karst area, northern China,

550   Environmental Earth Sciences, 75(1). https://doi. ARTN 51

551   10.1007/s12665-015-4869-6.

552 Kumar, A. R., Riyazuddin, P. 2012. Seasonal variation of redox species and redox

553   potentials in shallow groundwater: A comparison of measured and calculated

554   redox potentials. Journal of Hydrology, 444, 187-198. https://doi.

555   10.1016/j.jhydrol.2012.04.018.

556 Lawhon N. 2014. Investigating Telogenetic Karst Aquifer Processes and Evolution in

557   South-central Kentucky, U.S., Using High-resolution Storm Hydrology and

558   Geochemical Monitoring, MS in Geoscience, Department of Geography and

559   Geology, Western Kentucky University.

560   http://digitalcommons.wku.edu/theses/1324

561 Li, S. L., Liu, C. Q., Li, J., Lang, Y. C., Ding, H., Li, L. B. 2010. Geochemistry of

562   dissolved inorganic carbon and carbonate weathering in a small typical karstic

563   catchment of Southwest China: Isotopic and chemical constraints, Chemical

564   Geology, 277(3-4), 301-309, https://doi.10.1016/j.chemgeo.2010.08.013.

565 Li, T. Y., Li, H. C., Xiang, X. J., Kuo, T. S., Li, J. Y., Zhou, F. L., Chen, H. L., Peng, L.

566   L. 2012. Transportation characteristics of delta C-13 in the

567   plants-soil-bedrock-cave system in Chongqing karst area, Science China Earth

568   Sciences, 55(4), 685-694, https://doi.10.1007/s11430-011-4294-y.

569 Li, X., Blancheton, J. P., Liu, Y., Triplet, S., Michaud, L. 2014. Effect of

570   oxidation-reduction potential on performance of European sea bass

571   (Dicentrarchus labrax) in recirculating aquaculture systems. Aquaculture

572   International, 22(4), 1263-1282. https://doi.10.1007/s10499-013-9745-3.

573 Li, X. X., Wu, P., Han, Z. W., Zha, X. F., Ye, H. J., Qin, Y. J. 2018. Effects of mining

574   activities on evolution of water quality of karst waters in Midwestern Guizhou,

575   China: evidences from hydrochemistry and isotopic composition.

576   Environmental Science and Pollution Research, 25(2), 1220-1230.

577   https://doi.10.1007/s11356-017-0488-y.

578 Liao, H. K., Long, J., Li, J. 2015. Soil organic carbon associated in size-fractions as

579   affected by different land uses in karst region of Guizhou, Southwest China.

580   Environmental Earth Sciences, 74(9), 6877-6886.

581   https://doi.10.1007/s12665-015-4690-2

582 Liu, L. H., Shu, L. C., Chen, X. H., Oromo, T. 2010. The hydrologic function and

583   behavior of the Houzhai underground river basin, Guizhou Province, southwestern

584   China. Hydrogeology Journal, 18(2), 509-518.

585   https://doi.10.1007/s10040-009-0518-z.

586 Liu, X. Q., Wang, J., Zhang, D., Li, Y. T. 2009. Grey relational analysis on the relation

587   between marine environmental factors and oxidation-reduction potential. Chinese

588   Journal of Oceanology and Limnology, 27(3), 583-586.

589   https://doi.10.1007/s00343-009-9152-9

590 Liu, X. X., Yuan, S. H., Tong, M., Liu, D., 2017. Oxidation of trichloroethylene by the

591   hydroxyl radicals produced from oxygenation of reduced nontronite. Water

592   Research, 113, 72-79. https://doi. 10.1016/j.watres.2017.02.012

593   Liu, Z. H., Dreybrodt, W., Wang, H. J. 2010. A new direction in effective accounting

594   for the atmospheric CO2 budget: Considering the combined action of

595   carbonate dissolution, the global water cycle and photosynthetic uptake of DIC

596   by aquatic organisms. Earth-Science Reviews, 99(3-4), 162-172. https://doi.

597   10.1016/j.earscirev.2010.03.001

598   Lu, Y. R., 2007. Karst water resources and geo-ecology in typical regions of China.

599   Environmental   Geology,   51(5),   695-699.   https://doi.

600   10.1007/s00254-006-0381-3.

601   Luo, W. J., Wang, S. J. 2009. Transmission of delta C-13 signals and its paleoclimatic

602   implications in Liangfeng Cave system of Guizhou Province, SW China.

603   Environmental   Earth   Sciences,   59(3),   655-661.   https://doi.

604   10.1007/s12665-009-0062-0.

605   Macpherson, G. L., Roberts, J. A., Blair, J. M., Townsend, M. A., Fowle, D. A.,

606   Beisner, K. R. 2008. Increasing shallow groundwater CO2 and limestone

607   weathering, Konza Prairie, USA. Geochimica Et Cosmochimica Acta, 72(23),

608   5581-5599. https://doi. 10.1016/j.gca.2008.09.004

609   Marx, A., Conrad, M., Aizinger, V., Prechtel, A., van Geldern, R., Barth, J. A. C. 2018.

610   Groundwater data improve modelling of headwater stream CO2 outgassing

611   with a stable DIC isotope approach. Biogeosciences 15, 3093-3106. https://doi.

612   10.5194/bg-15-3093-2018.

613   McClanahan, K., Polk, J., Groves, C., Osterhoudt, L., Grubbs., S. 2016. Dissolved

614   inorganic carbon sourcing using C-13(DIC) from a karst influenced river

system, Earth Surface Processes and Landforms, 41(3), 392-405. https://doi.10.1002/esp.3856.

McGee, D. K., Wynn, J. G., Onac, B. P., Harries, P. J., Rothfus, E. A. 2010. Tracing groundwater geochemistry using delta C-13 on San Salvador Island (southeastern Bahamas): implications for carbonate island hydrogeology and dissolution, Carbonates and Evaporites, 25(2), 91-105. https://doi.10.1007/s13146-010-0013-6.

Mondal, N. C., Singh, V. P., Singh, V. S., Saxena, V. K. 2010. Determining the interaction between groundwater and saline water through groundwater major ions chemistry. Journal of Hydrology, 388(1-2), 100-111. https://doi.10.1016/j.jhydrol.2010.04.032

Phillips, D. L., Gregg, J. W. 2003. Source partitioning using stable isotopes: coping with too many sources, Oecologia, 136(2), 261-269. https://doi.10.1007/s00442-003-1218-3.

Rouw, A., Soulileuth, D., Huon, B. S. 2015. Stable carbon isotope ratios in soil and vegetation shift with cultivation practices (Northern Laos), Agriculture Ecosystems & Environment, 200, 161-168. https://doi.10.1016/j.agee.2014.11.017

Schulte, P., van Geldern, R., Freitag, H., Karim, A., Negrel, P., Petelet-Giraud, E., Barth, J. A. C. 2011. Applications of stable water and carbon isotopes in watershed research: Weathering, carbon cycling, and water balances. Earth-Science Reviews, 109(1-2), 20-31.

637   https://doi.10.1016/j.earscirev.2011.07.003.

638   Shin, W. J., Chung, G. S., Lee, D., & Lee, K. S. 2011. Dissolved inorganic carbon

639   export from carbonate and silicate catchments estimated from carbonate

640   chemistry and $\delta 13CDIC$, Hydrology & Earth System Sciences, 15(8),

641   2551-2560. https://doi.10.5194/hessd-8-1799-2011.

642   Song, X. W., Gao, Y., Wen, X. F., Guo, D. L., Yu, G. R., He, N. P., Zhang, J. Z. 2017.

643   Carbon sequestration potential and its eco-service function in the karst area,

644   China. Journal of Geographical Sciences, 27(8), 967-980.

645   https://doi.10.1007/s11442-017-1415-3.

646   Stallard, R. F., Edmond, J. M. 1983. Geochemistry of the Amazon .2. The Influence of

647   Geology and Weathering Environment on the Dissolved-Load. Journal of

648   Geophysical Research-Oceans, 88(Nc14), 9671-9688.

649   https://doi.10.1029/Jc088ic14p09671.

650   Tallini, M., Falcone, R. A., Carucci, V., Falgiani, A., Parisse, B., Petitta, M. 2014.

651   Isotope hydrology and geochemical modeling: new insights into the recharge

652   processes and water-rock interactions of a fissured carbonate aquifer (Gran

653   Sasso, central Italy), Environmental Earth Sciences, 72(12), 4957-4971,

654   https://doi.10.1007/s12665-014-3364-9.

655   Tobias, C., Bohlke, J. K. 2011. Biological and geochemical controls on diel dissolved

656   inorganic carbon cycling in a low-order agricultural stream: Implications for

657   reach scales and beyond. Chemical Geology, 283(1-2), 18-30.

658   https://doi.10.1016/j.chemgeo.2010.12.012.

659   van Geldern, R., Schulte, P., Mader, M., Baier, A., Barth, J. A. C. 2015. Spatial and

660   temporal variations of pCO(2), dissolved inorganic carbon and stable isotopes

661   along a temperate karstic watercourse, Hydrological Processes, 29(15),

662   3423-3440. https://doi.10.1002/hyp.10457.

663   Wang, G., Feng, X., Han, J., Zhou, L., Tan, W., Su, F. 2008. Paleovegetation

664   reconstruction using delta C-13 of Soil Organic Matter. Biogeosciences, 5(5),

665   1325-1337. https://doi. 10.5194/bg-5-1325-2008.

666   Wang, Y. F., Chen, L. D., Gao, Y., Chen, S. B., Chen, W. L., Hao, Z., Jia, J .J., Han, N.,

667   2017a. Geochemical isotopic composition in the Loess Plateau and

668   corresponding source analyses: A case study of China's Yangjuangou

669   catchment. Science of the Total Environment, 581, 794-800.

670   https://doi.10.1016/j.scitotenv.2017.01.012.

671   Wang, Z. M., Rawal, K., Hu, L. B., Yang, R. D., Yang, G. L., 2017b. A study of

672   dissolution and water-bearing characteristics of the restricted platform

673   dolomite facies in the karst areas of Guizhou, China. Environmental Earth

674   Sciences, 76(3). https://doi. Artn 12410.1007/S12665-017-6419-X.

675   Williams P. W., Fong, Y. T., 2010. Karst Regions of the World. Circle of Blue online

676   at:http://www.circleofblue.org/waternews/wp-content/uploads/2010/01/world-

677   karst-map-web-1.12.jpg, (Accessed March 29, 2013).

678   Wynn, J. G., Harden, J. W., Fries, T. L. 2006. Stable carbon isotope depth profiles and

679   soil organic carbon dynamics in the lower Mississippi Basin. Geoderma,

680   131(1-2), 89-109. https://doi.10.1016/j.geoderma.2005.03.005.

681   Yan, J. H., Li, J. M., Ye, Q., Li, K. 2012. Concentrations and exports of solutes from

682   surface runoff in Houzhai Karst Basin, southwest China, Chemical Geology,

683   304, 1-9. https://doi.10.1016/j.chemgeo.2012.02.003.

684   Yan, J. H., Wang, W. T., Zhou, C. Y., Li, K., Wang, S. J. 2014. Responses of water

685   yield and dissolved inorganic carbon export to forest recovery in the Houzhai

686   karst basin, southwest China, Hydrological Processes, 28(4), 2082-2090.

687   https://doi.10.1002/hyp.9761.

688   Ye, F., Guo, W., Shi, Z., Jia, G. D., Wei, G. J., 2017. Seasonal dynamics of particulate

689   organic matter and its response to flooding in the Pearl River Estuary, China,

690   revealed by stable isotope (delta C-13 and delta N-15) analyses. J Geophys

691   Res-Oceans 122, 6835-6856. https://doi. 10.1002/2017JC012931.

692   Zeng, C., Liu, Z. H., Yang, J. W., Yang, R. 2015. A groundwater conceptual model and

693   karst-related carbon sink for a glacierized alpine karst aquifer, Southwestern

694   China, Journal of Hydrology, 529, 120-133.

695   https://doi.10.1016/j.jhydrol.2015.07.027.

696   Zhao, M., Liu, Z. H., Li, H. C., Zeng, C., Yang, R., Chen, B., Yan, H. 2015. Response

697   of dissolved inorganic carbon (DIC) and delta C-13(DIC) to changes in

698   climate and land cover in SW China karst catchments. Geochimica Et

699   Cosmochimica Acta, 165, 123-136. https://doi. 10.1016/j.gca.2015.05.041.

700   Zhao, M., Zeng, C., Liu, Z. H., Wang S. J. 2010. Effect of different land use/land

701   cover on karst hydrogeochemistry: A paired catchment study of Chenqi and

702   Dengzhanhe, Puding, Guizhou, SW China, Journal of Hydrology, 388(1-2),

703   121-130. https://doi.10.1016/j.jhydrol.2010.04.034.

704

Table 1 Water quality parameters of surface water, groundwater and mixed water in

Houzhai and Chenqi.

Sample	Summer				Autumn			
	COND	TDS	ORP		COND	TDS	ORP	
Point				PH				PH
	(uS cm^{-1})	(mg.L^{-1})	(mv)		(uS cm^{-1})	(mg.L^{-1})	(mv)	
HZ-S	410	276	216	7.9	391	262	187	8.6
HZ-G	397	266	219	7.9	423	285	186	8.8
HZ-M	403	271	216	8.3	456	308	181	8.8
CQ-S	452	510	213	9.0	836	581	124	8.9
CQ-G	491	586	194	9.0	780	542	130	9.0
CQ-M	747	514	203	9.0	1042	723	134	8.9
Sample	Winter				Spring			
	COND	TDS	ORP		COND	TDS	ORP	
Point				PH				PH
	(uS cm^{-1})	(mg.L^{-1})	(mv)		(uS cm^{-1})	(mg.L^{-1})	(mv)	
HZ-S	396	266	211	8.4	467	315	208	8.3
HZ-G	451	304	212	8.5	635	432	219	8.2
HZ-M	405	272	211	8.5	626	426	223	8.3
CQ-S	770	526	125	8.9	838	573	218	7.9
CQ-G	740	514	127	9.1	855	596	217	8.1
CQ-M	787	557	122	9.1	896	615	217	8.2

707   (Note: pH, COND, TDS and ORP were measured by Ultrameter II (Myron L company USA.
708   HZ-S values represent the average for all the surface water points (No. 1 through No. 10) in the
709   Houzhai watershed; HZ-G values represent the average for No.1G in different months; HZ-M
710   values represent the average for No.1M in different months. CQ-G values represent the average of
711   the four groundwater sampling points in different months; CQ-S values represent the average of
712   the six surface water sampling points in different months and CQ-M values represent the average
713   for the No.7 in different months.)

714

715

716

Table 2 Seasonal trends of model results for Chenqi and Houzhai

718

		Ground water		Atmosphere deposition		Soil water		Carbonate reaction	
		value	median standard	value	median standard	value	median standard	value	median standard
(Chenqi)	Median	28%	23%	18%	15%	9%	8%	38%	13%
Summer	Minimum	0%		0%		0%		6%	
	Maximum	94%		60%		31%		69%	
	Median	32%	24%	20%	16%	11%	9%	29%	14%
Fall	Minimum	0%		0%		0%		0%	
	Maximum	93%		64%		37%		61%	
(Houzhai)	Median	29%	23%	18%	15%	10%	8%	36%	13%
Fall	Minimum	0%		0%		0%		4%	
	Maximum	95%		61%		34%		65%	
	Median	30%	25%	17%	14%	9%	8%	36%	15%
Winter	Minimum	0%		0%		0%		0%	
	Maximum	97%		57%		30%		67%	
	Median	32%	24%	17%	13%	10%	8%	36%	16%
Spring	Minimum	0%		0%		0%		0%	
	Maximum	92%		53%		31%		66%	

(Note: 719 IsoSource calculation automatic generated results. Groundwater, atmosphere deposition, soil water and carbonate 720 reactions as the four sources of river water in this study. The median, minimum and maximum of possibility within 721 the river routinely produced and median standard contributions of 20–25% and 8–16%, respectively).

722

723

724

725

726

727

728

729

730

Table 3 Cations and anions concentrations of surface water, groundwater in Houzhai and Chenqi.

Points Concentrations ($mmol \cdot L^{-1}$)	Summer				Autumn			
	CQ-S	CQ-G	HZ-S	HZ-G	CQ-S	CQ-G	HZ-S	HZ-G
Ca^{2+}	4.55	2.86	1.06	1.28	6.73	2.89	1.74	1.01
Mg^{2+}	2.17	1.13	0.83	0.91	3.38	1.33	0.96	0.87
Na^+	0.29	0.08	0.13	0.15	0.32	0.09	0.19	0.16
K^+	0.38	0.06	0.07	0.07	0.13	0.05	0.11	0.08
SO_4^{2-}	1.36	2.97	0.60	0.60	2.68	1.31	0.90	0.60
Cl^-	0.15	0.19	0.19	0.30	0.18	0.22	0.25	0.21
HCO_3^-	0.45	0.45	0.51	0.57	0.39	0.41	0.54	0.50
SiO_2	0.19	0.14	0.02	0.05	0.28	0.14	0.09	0.07
season	Winter				Spring			
Point	CQ-S	CQ-G	HZ-S	HZ-G	CQ-S	CQ-G	HZ-S	HZ-G
Ca^{2+}	2.44	2.64	1.19	1.00	3.41	3.34	2.25	1.98
Mg^{2+}	1.16	1.38	0.78	0.86	1.30	1.74	1.23	1.19
Na^+	0.07	0.09	0.21	0.20	0.15	0.59	0.37	0.54
K^+	0.03	0.03	0.10	0.05	0.16	0.06	0.15	0.07
SO_4^{2-}	1.97	2.61	1.19	0.77	3.10	2.44	1.61	0.99
Cl^-	0.17	0.11	0.31	0.31	0.23	0.13	0.39	0.39
HCO_3^-	0.39	0.44	0.52	0.57	0.55	0.55	0.56	0.58
SiO_2	0.13	0.14	0.06	0.06	0.17	0.15	0.05	0.06

733 (Note: HZ-S values represent the average for all the surface water points (No. 1 through No. 10) in
734 the Houzhai watershed; HZ-G values represent the average for No.1G in different months. CQ-G
735 values represent the average of the four groundwater sampling points in different months; CQ-S
736 values represent the average of the six surface water sampling points in different months.)

737

738

739

740

741

742

743

744

745

Figure Caption

Figure 1 (a) Study sites location in Puding County, Guizhou. (b) The water sampling

points in Houzhai watershed. (c) The water sampling points in Chenqi catchment. (d)

The soil sampling points in Chenqi catchment.

Figure 2 (a) The seasonal variation of pH values in Houzhai. (b) The seasonal

variation of pH values in Chenqi.(c) Correlation between pH with water quality

parameters of atmospheric deposition from 2016 to 2017.

Figure 3(a) Variation of [DIC] of rainfall during 2016 to 2017. (b) The variation of

$\delta^{13}C_{DIC}$ of rainfall during 2016 to 2017.

Figure 4 (a) The seasonal variation of DIC in Houzhai watershed. (b) The seasonal

variation of DIC in Chenqi catchment. (c) Seasonal variation of $\delta^{13}C$ values in

Houzhai watershed. (d) The variation of $\delta^{13}C$ values in surface water and groundwater

in Chenqi catchment.

Figure 5(a) The $\delta^{13}C$ values of soil collected at four different locations (A to D) on

Tianlong Mountain. The $\delta^{13}C$ values of two transects of a ditch between two hills with

four depths in Chenqi (b) CQ-1 and (c) CQ-2.

Figure 6 (a) The $\delta^{13}C$ values of arbor plants in Tianlong Mountain. (b) The $\delta^{13}C$ values

of leaves, twig and roots of tree in Chenqi.

Figure 7 Season series analysis of mixing model results for Chenqi and Houzhai.

Figure 8 The Piper diagram of cationic and anion in surface water and groundwater in

Chenqi and Houzhai watershed.

Figure 9 Component loadings of principal component analysis of Chenqi and Houzhai

watershed

769   Figure 10 ^{13}C cycle in a nested karst watershed and proportion of carbon sources in the

770   river.

771

772

773

774   **Figure 1**
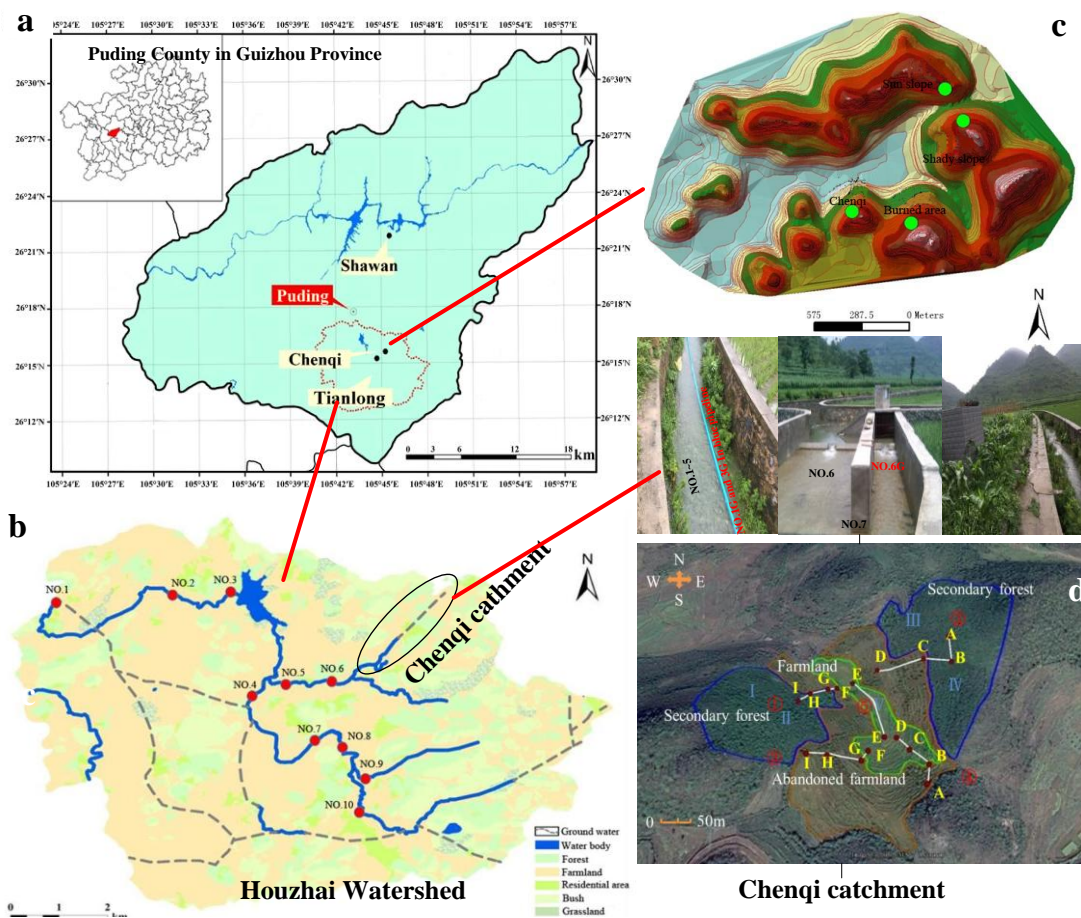
775

776

777

778

779

780

781

782

783
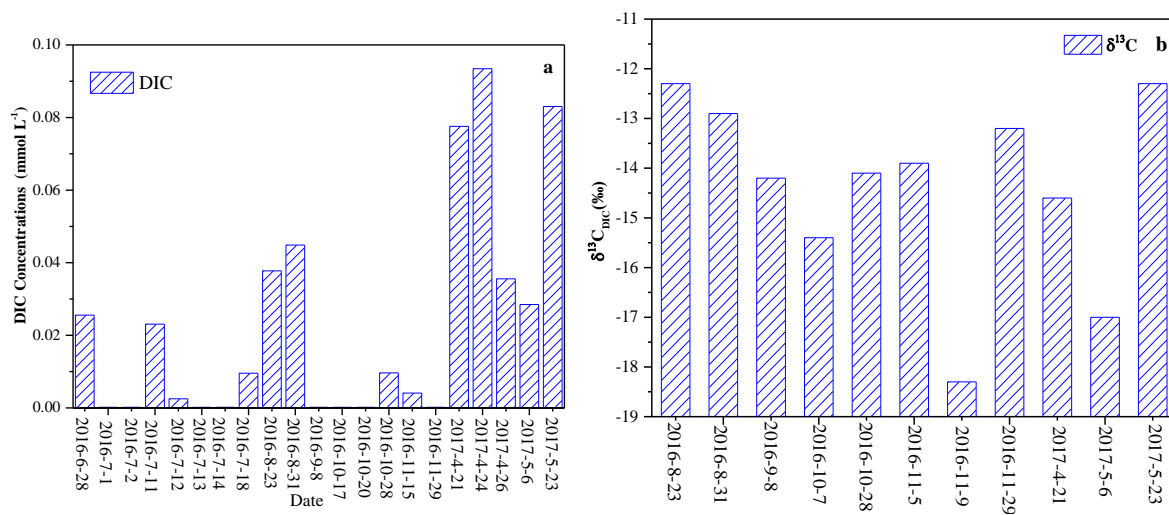
784

785
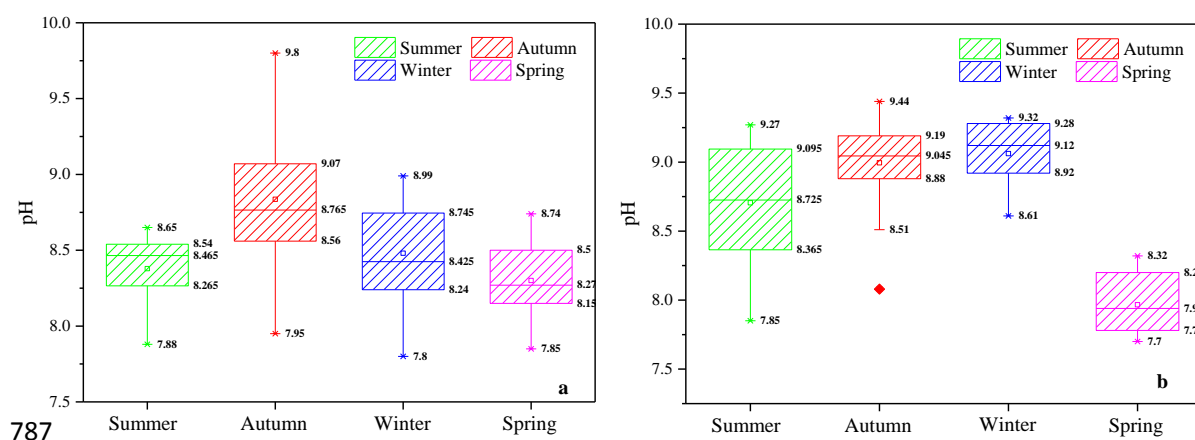
Figure 2

787
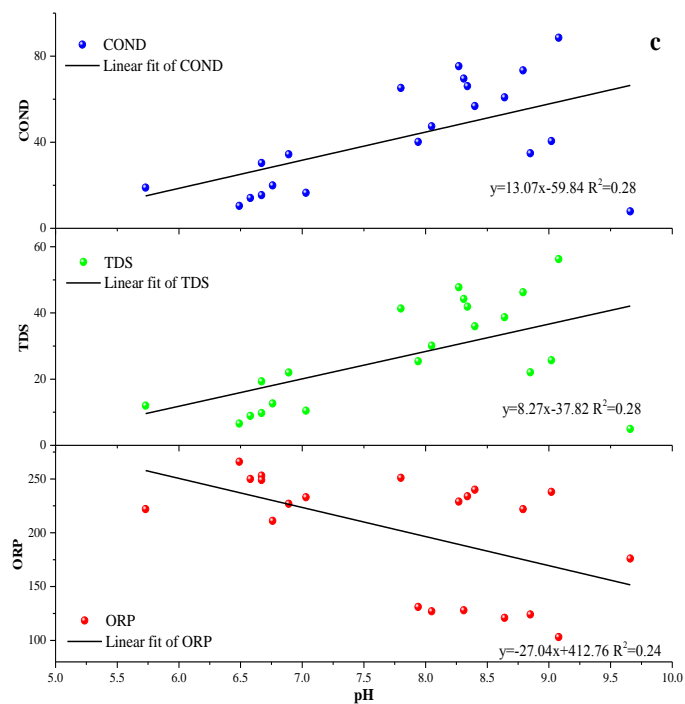
788

789

790

791

792

793

794

795

Figure 3

797

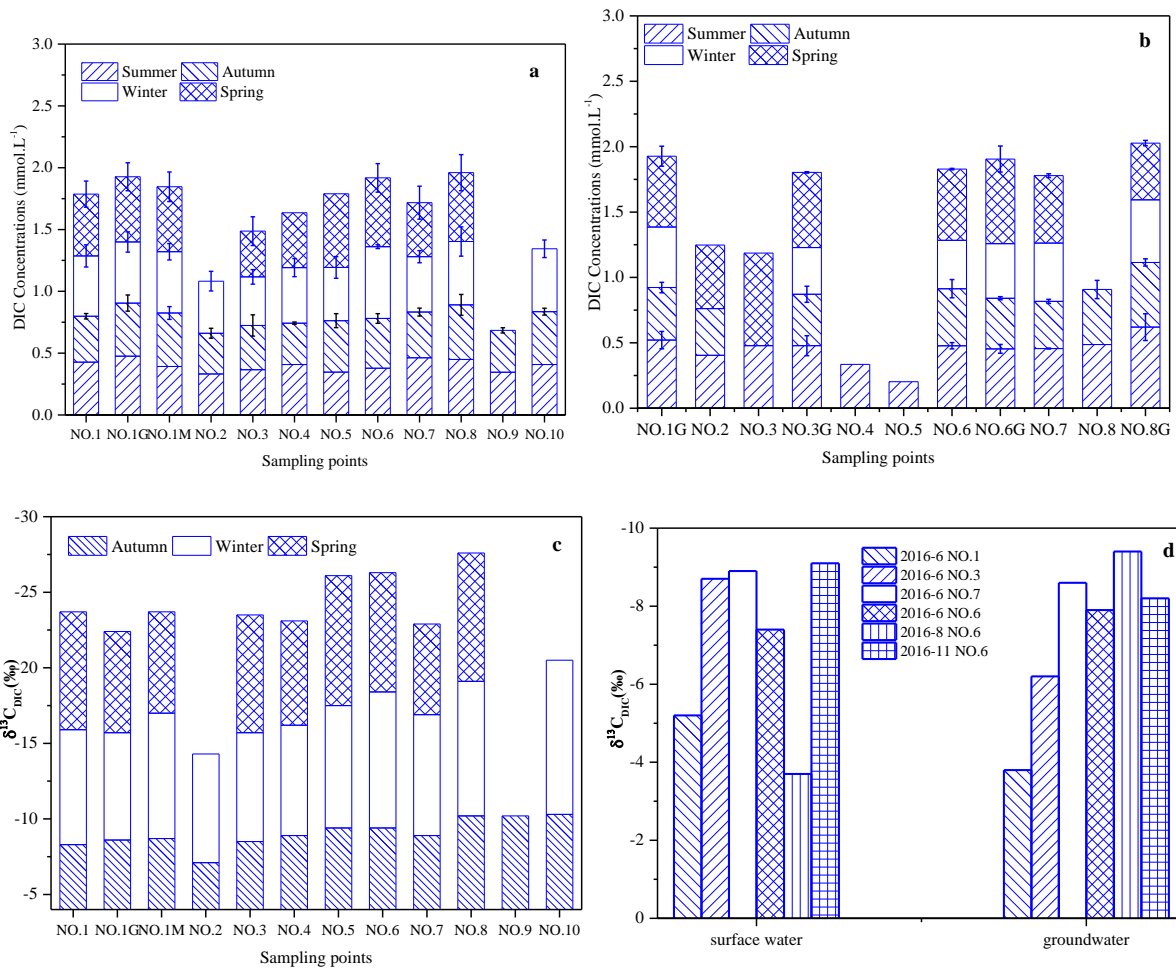
798

799

800

801

802

803

804

805

806

807

808

809

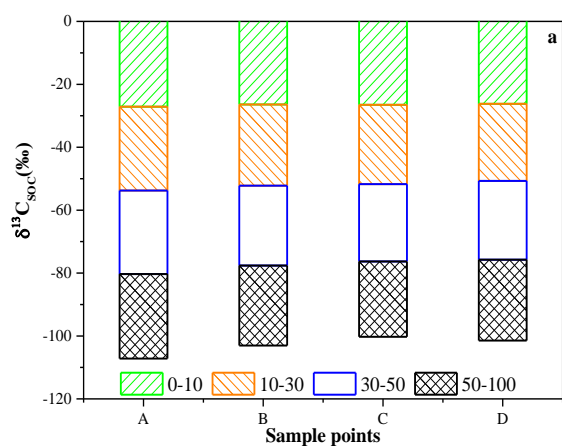810

811

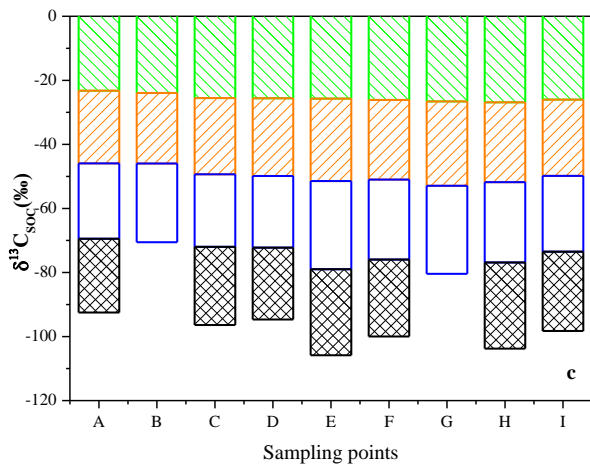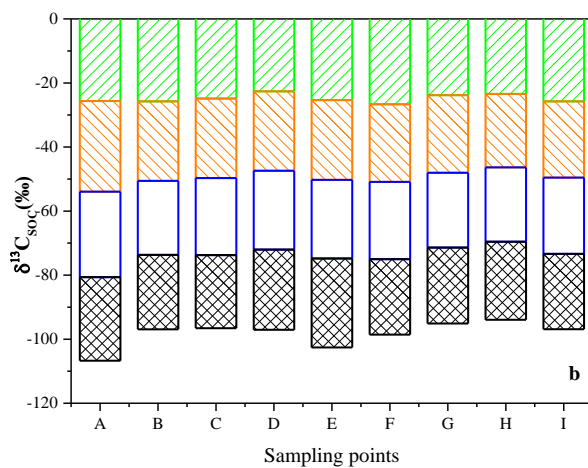**Figure 4**

813

814

815

816

817

818

819

820

821

822

823

Figure 5

825

826

827

828

829

830

831

832

833

834

835

836

Figure 6

838

839

840
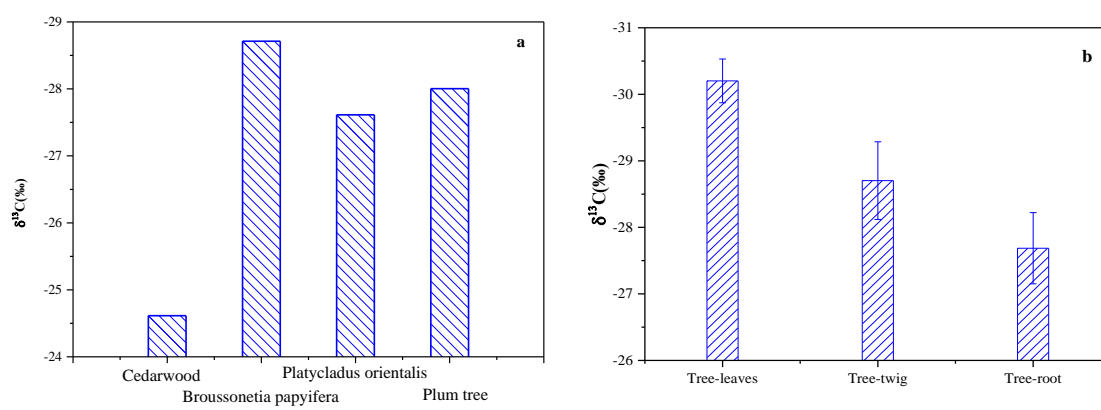
841

842

843

844

845

846

847

848

849

850

851

852

853

854

855

856

857   **Figure 7**

858
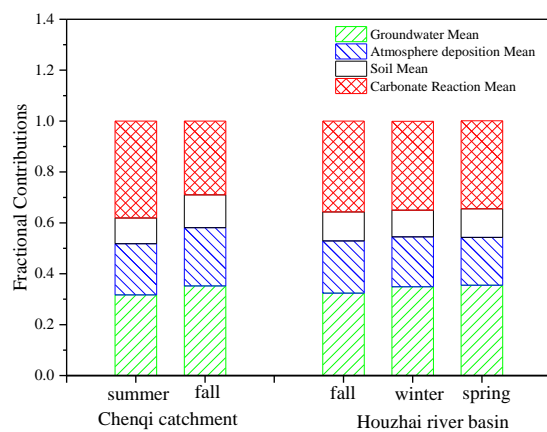
859
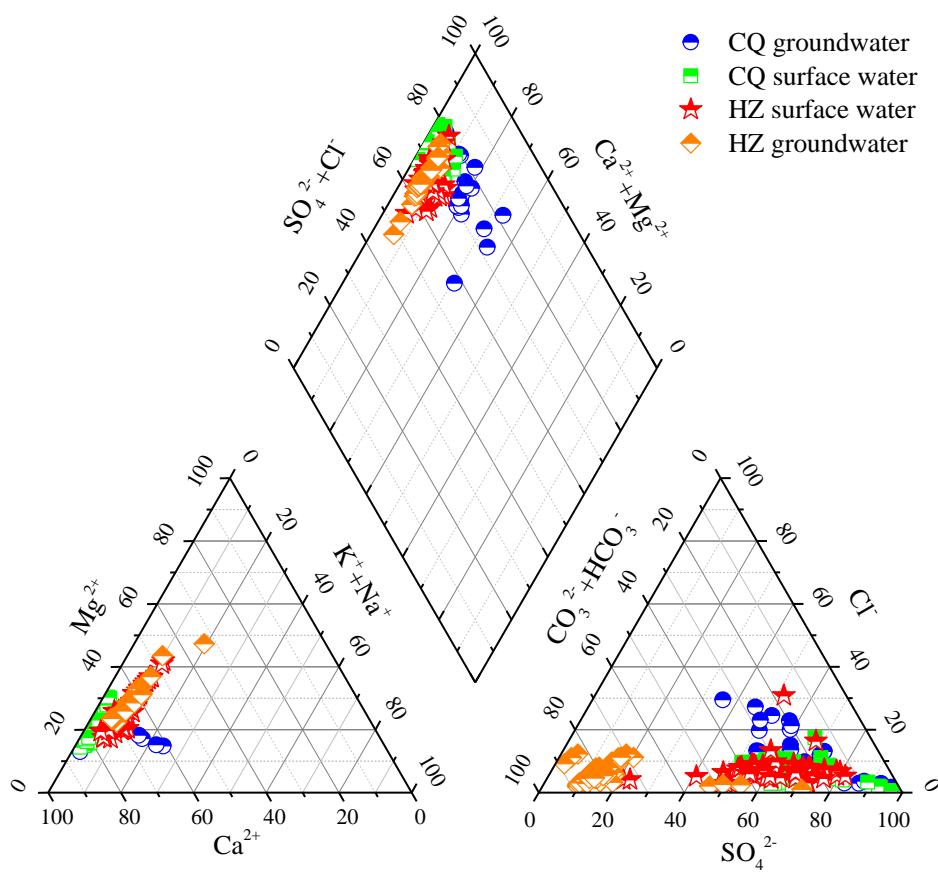
860

861

862

863

864

865

866

867

868

869

870

871

872

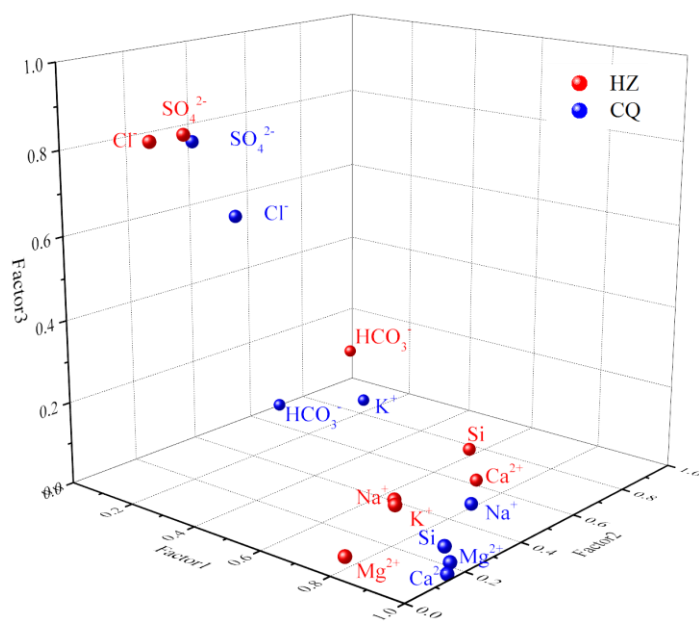873

Figure 8

875

876

877

878

879

880

881

882

883

884

885

Figure 9

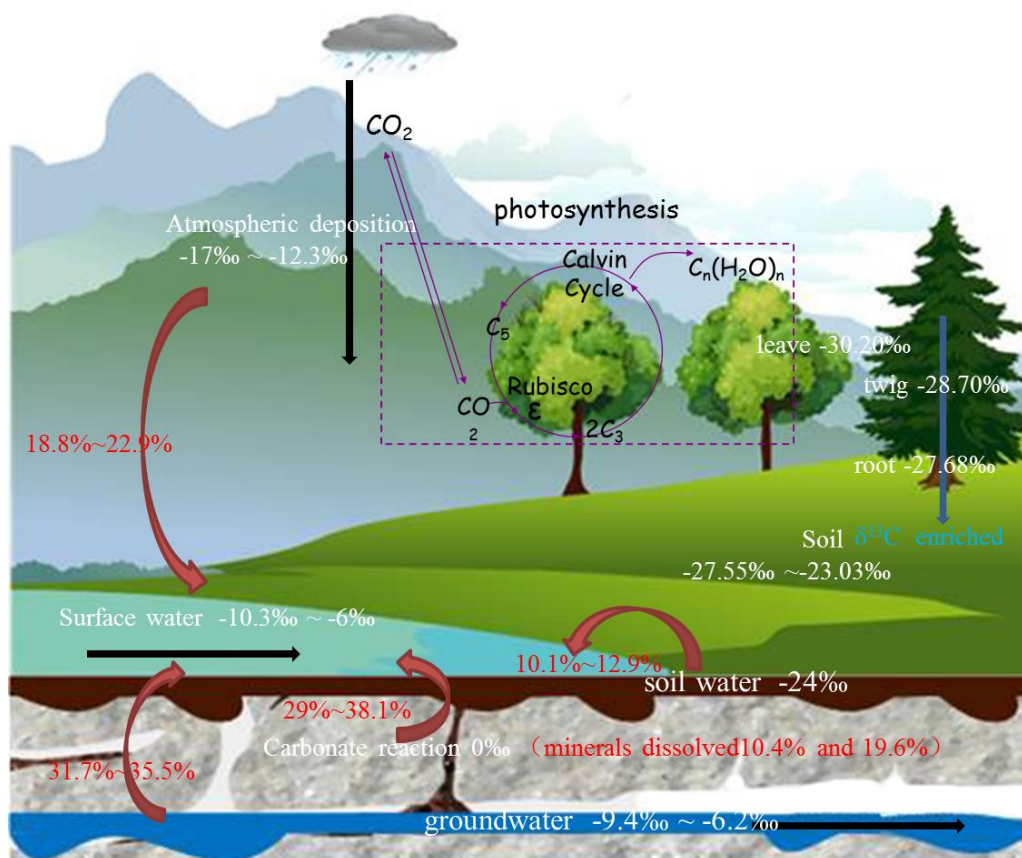887

888
889

890

891

892

893

894

895

896

897

898

899

900

901

Figure 10

903

904

905

906

907